Numerical modeling of the constriction of the dc positive column in rare gases

G. M. Petrov and C. M. Ferreira
Centro de Física de Plasmas, Instituto Superior Técnico, 1096 Lisboa Codex, Portugal
(Received 7 January 1998; revised manuscript received 16 June 1998)

The constriction of the positive column of a dc glow discharge in argon at high pressures is analyzed using the continuity equations for the charged particles and the gas thermal balance equation coupled with the local electron Boltzmann equation and a detailed collisional-radiative model for the atomic and ionic species. Contrary to the other existing models of the constriction in inert gas, the present model is self-consistent and fully detailed, and provides a quantitative description of all the discharge properties. The numerical techniques used to solve the boundary value problem corresponding to our set of equations are discussed in detail. The transition from the diffuse to the constricted state and the properties of this latter state are investigated. The model predicts the existence of multimodal solutions for the discharge parameters as a function of the discharge specific power, within a limited range of values of the latter above a critical value, which explains the observed abrupt changes in the discharge parameters and the hysteresis associated with constriction. The radial distributions of the gas temperature and of the densities of all neutral and charged species considered are determined along with various other discharge characteristics, such as the steady-state discharge maintenance electric field, as a function of the discharge operating parameters. The results for argon show satisfactory agreement with data from experiments. A few model simulations are further presented that enable one to gain physical insight on the relevant kinetic processes of constriction in argon. Such simulations are instrumental to understanding also the mechanisms of constriction in the other inert gases. [S1063-651X(99)11703-3]

PACS number(s): 52.80.−s, 51.50.+v, 52.20.Fs, 52.20.Hv

I. INTRODUCTION

At intermediate gas pressures typically below 10 Torr the positive column of a glow discharge is usually diffuse, filling the whole cross section of the discharge tube. The radial distribution of the electron and ion densities can be described as a first approximation by the Shottky diffusion theory, eventually with corrections accounting for stepwise ionization effects. Accurate calculations show that this distribution is usually close to the J_0-Bessel function. At higher pressures, however, the discharge is likely to contract around the tube axis, forming a bright narrow filament. This well-defined constricted discharge mode, which exists at pressures from a few Torr to about 1 atm, can neither be classified as a thermal arc nor as a classical ''cold'' discharge; thus it falls into an intermediate category.

There have been many theoretical [1–13] and experimental [1–3,13–15] investigations of constricted discharges in inert gases that have shown that the constriction arises above a certain critical pressure. However, the onset of this constriction depends also on the tube radius R and the discharge current I. In particular, the experiments have revealed that the critical value pR for Ar is approximately 20 Torr cm [13]. Below the critical pressure the discharge exists in a diffuse state, filling the whole tube cross section. Above the critical pressure it may exist either in a diffuse or a contracted state, depending on whether the current is below or above a critical value, respectively. Therefore, the constriction occurs if both the discharge current and the pressure exceed their critical values. The transition from the diffuse to the constricted mode occurs abruptly and is accompanied by a sudden increase of the electron density at the discharge axis by more than an order of magnitude. At the transition, all the internal plasma parameters change discontinuously and show hysteresis, that is, the transition from the diffuse to the contracted state (with increasing current) and the reverse transition (with decreasing current) occur at different values of the discharge parameters [10,14].

Discharge constriction in inert gases has also been observed in microwave discharges, such as, for example, surface wave discharges at high pressures [16,17]. It can be expected that the basic mechanisms causing constriction are essentially the same in the ordinary dc positive column and the microwave discharge, but a common theory for both cases is still lacking at present. Although this paper is mainly concerned with dc discharges, it will be shown that the present formulation can be extended to microwave discharges also.

The constriction phenomenon occurs not only in inert gases. It takes place in molecular and in electronegative gases too [18–21], but the numerical models required for such gases are somewhat different from those for inert gases due to the presence of molecules and/or negative ions. Therefore, we will not be concerned with molecular or electronegative gases here.

Several theories based on somewhat crude analytical approaches have formerly been developed to explain the causes of constriction in inert gases. These theories fall essentially into two different categories. One category includes those theories in which an explanation of constriction is sought as a direct consequence of nonuniform gas heating across the discharge [1–3,13]. In most theories of this type the contraction is attributed to the effects of the gas temperature radial gradient on the local ionization-recombination balance of the charged particles. To describe such effects some authors [3,13] adopted formulations based upon the classical theory

of thermal arcs. Others have rather focused on the radial variation of the recombination rate. Assuming that the temperature in the central region is high enough for the molecular ions to be efficiently dissociated, it was suggested that an increased dissociative recombination rate towards the cooler outer regions could result in a rapid loss of charged particles and thus account quite generally for constriction [1]. One of the drawbacks of the theories just described is their neglect of diffusion in the charged particle balance, since large gradients in the electron density are associated with contraction. In particular, the charged particle balance cannot be transformed to a local balance in those cases in which the ionization rate drops fast enough radially to become smaller than the recombination rate. For this reason, another category of theories, generally termed diffusion-recombination theories, have been proposed in the literature [4,6–12]. According to such theories, constriction is caused by rapid radial variations in the net volumetric source term, the difference of the rates of ionization, and electron-ion recombination. On axis, the net volumetric source is positive. In the outer regions, this source is negative. Continuity is maintained in the outer region through a diffusion-recombination balance. The reason why the net volumetric source changes sign is the rapid radial decrease of the ionization rate due to the strongly nonlinear dependence of this rate on the degree of ionization [4,10–12] through stepwise ionization processes and the influence of electron-electron collisions on the shape of the electron energy distribution function. In particular, Golubovskii and co-workers [10–12] have found that the most important reason for the discontinuous contraction in inert gases (except helium) is the nonlinear dependence of the ionization rate on the electron density through the above electron-electron collision effects. According to these authors, when such collisions are neglected in the theory (as in [4]) contraction still occurs but without a discontinuous character. Further, nonuniform heating of the gas has not been found in [10–12] to be a determining factor, but to cause only additional contraction and a shift of the critical pressure and current towards lower values.

The major weakness of all the theories mentioned above lies in their semiquantitative nature and limited accuracy, since the discharge kinetics is not treated in a consistent way in any of them. Due to the complex discharge kinetics occurring at pressures of tens or hundreds of Torr, it is clear that the discharge properties cannot be correctly described using, for example, analytical expressions for the ionization and recombination rates, or for the number densities of atomic ions, molecular ions, and populations of the excited states. For this reason, it is difficult to ascertain which theories are right or wrong, and why. There is therefore a need to develop a more accurate theory capable of providing a deeper insight into the relevant kinetic processes of discharge constriction. A proper description can only be achieved by coupling the particle balance equations for all relevant charged and neutral species to the electron Boltzmann equation and the gas thermal balance equation. In fact, the densities of the charged particles and the excited species, and the ionization and the recombination rates can only be correctly determined in the framework of an accurate model for the species kinetics and transport in which all the electron rate coefficients and transport parameters are determined from the solution to the electron Boltzmann equation. The development of a model of this kind to investigate the constriction phenomenon is the main purpose of this work. We have chosen argon as a working example but some results of this work can be extended to the other rare gases with proper adaptations.

The organization of this paper is the following. In Sec. II we present the basic differential equations to be solved in order to understand the constriction problem, namely, the electron continuity equation and the gas thermal balance equation, and we discuss the appropriate boundary conditions for these equations. In Sec. III the kinetic model and the set of plasmochemical reactions taken into account are briefly presented. The numerical approach used to solve the whole set of equations of our model is discussed in Sec. IV. An analysis of the discharge properties under both the diffuse and the constricted regimes and of the transition between these regimes is given in Sec. V. In particular, calculations of the electron energy distribution function, the densities of all charged species, and the populations of the excited states as a function of the radius, as well as calculations of other important discharge characteristics for various pressures and discharge currents, are presented and analyzed. It is shown that the model predictions agree satisfactorily with experiments. A detailed analysis of the various mechanisms causing constriction and of their effects is also carried out. Finally, Sec. VI summarizes the principal conclusions of this investigation.

II. STATEMENT OF THE PROBLEM

The discharge column is considered to be cylindrically symmetric and longitudinally uniform. Our main purpose here is to determine the electron density distribution $n_e(r)$, the gas temperature distribution $T_g(r)$, and the maintaining electric field E, which is assumed to be uniform, as a function of the discharge operating parameters, namely, the gas pressure p, the discharge current I, and the tube radius R. The distributions $n_e(r)$ and $T_g(r)$ can be obtained from a closed system of macroscopic equations consisting of the continuity equation for the electrons, the heat transport equation for the gas, and the equation of state for the gas pressure [5–12]. These equations must of course be complemented with appropriate kinetic equations determining the local net sources of electrons and of gas heating within the plasma volume. The above system of macroscopic equations and the boundary conditions they must satisfy is considered below, for a steady-state discharge.

The electron continuity equation can be written as

$$-\frac{1}{r}\frac{d}{dr}\left(rD_a\frac{dn_e}{dr}\right)=\Gamma_{\mathrm{ion}}-\Gamma_{\mathrm{rec}}, \tag{1}$$

where D_a is the ambipolar diffusion coefficient; Γ_{ion} and Γ_{rec} are, respectively, the total number of ionization and recombination events per unit volume and unit time. This is a second-order differential equation that can be directly integrated if its right-hand side is known. The right-hand side of this equation, as well as the ambipolar diffusion coefficient, can be obtained from the electron Boltzmann equation coupled to a collisional-radiative model for the argon plasma

as discussed in Sec. III. It must be stressed at this point that both the ionization and the recombination rates depend on the four parameters N, n_e, E, and T_g, that is,

$$\Gamma_{\text{ion}}=\Gamma_{\text{ion}}(N,n_e,E,T_g), \tag{2}$$

$$\Gamma_{\text{rec}}=\Gamma_{\text{rec}}(N,n_e,E,T_g). \tag{3}$$

The right-hand side of Eq. (1) is usually positive in a diffuse discharge ($\Gamma_{\text{rec}}\ll\Gamma_{\text{ion}}$), while it can change sign at some intermediate radial position in the case of a constricted discharge. Both Γ_{rec} and Γ_{ion} depend strongly on the electron density. The nonlinear dependence of Γ_{ion} on the electron density is caused both by multistep ionization processes and electron-electron collision effects. Several authors [4,10–12] have considered this nonlinearity as the main cause of contraction. As is well known, the ambipolar diffusion coefficient depends in a complex way on the relative densities of the various ionic species present and their corresponding mobilities, and on the electron mobility and free diffusion coefficient. It must be determined from the electron Boltzmann equation and the collisional-radiative model.

The appropriate boundary conditions for Eq. (1) under the present conditions are

$$\frac{dn_e(0)}{dr}=0, \quad n_e(R)=0. \tag{4}$$

Gas heating in the discharge leads to a nonuniform distribution of the neutral atoms across the radius, with a depletion of the atom density in the central region. Assuming that heat conduction is the predominant cooling mechanism, the radial distribution of the gas temperature can be found by solving the following gas thermal balance equation:

$$-\frac{1}{r}\frac{d}{dr}\left(r\kappa(T_g)\frac{dT_g}{dr}\right)=Q(r), \tag{5}$$

where κ is the thermal conductivity, which is a function of the gas temperature for most gases. For argon, $\kappa=4.17\times10^{-6}T_g^{2/3}$ W/(cm deg$^{5/3}$) [14]. The term $Q(r)$ on the right-hand side of this equation accounts for all the gas heating sources occurring in the volume. It has been assumed in [10,12] that all the deposited power in the discharge is dissipated in gas heating, in which case $Q(r)=Ej(r)$, where $j(r)$ is the current density. Since power is also dissipated in many other processes, such as ionization and excitation of metastable and radiative states, the above assumption can be a crude overestimation. An accurate determination of $Q(r)$ requires detailed kinetic calculations as performed here using our collisional-radiative model and the electron Boltzmann equation.

The appropriate boundary conditions for Eq. (5) are

$$\frac{dT_g(0)}{dr}=0, \quad T_g(R)=T_w. \tag{6}$$

The gas temperature at the wall T_w has been assumed to be 300 K in all our calculations, since this was the value of the wall temperature in the experiments considered below for comparison.

The atom density N is connected with the gas temperature and pressure through the equation of state

$$N(r)=\frac{p}{k_BT_g(r)}, \tag{7}$$

where k_B is the Boltzmann constant.

Equations (1), (5), and (7), with the boundary conditions (4) and (6), together with the plasma kinetic equations of Sec. III constitute a closed system of equations determining the radial distribution of all discharge characteristics of interest, such as gas temperature, atom, electron and ion densities, excited states populations, electron and ion mobilities, electron diffusion coefficient, mean energy, and all rate constants for elementary processes.

III. KINETIC MODEL

As stated above, a detailed description of the discharge kinetics must be achieved in order to solve the constriction problem accurately. The kinetic model that is needed must provide a complete and self-contained description of the discharge properties at high pressure-radius products (typically above 100 Torr cm) and degrees of ionization up to 10^{-2}. Note that several other models for Ar have previously been proposed in the literature. These include, for example, an analytical model [22], a model for electron-beam generated plasmas [23,24], models applicable at low pressures [25], or at high pressures [26,27], and models taking into account highly excited Ar states [28,29]. However, none of these models is applicable here for one reason or another, for example, either because they do not include highly excited Ar states, or the heavy-particle kinetics, or (excepting [26,27]) the formation of Ar_2^* dimers.

For this reason, we have developed a detailed collisional-radiative model for an argon plasma at high pressures that takes into account the following species: Ar (ground-state atoms), Ar($4s$), Ar($4p$), Ar($3d$), Ar($5s$), Ar($5p$), Ar($4d$), Ar($6s$), Ar_2^* (excited dimers), Ar^+, Ar_2^+, and Ar_3^+. All excited states belonging to the same configuration have been lumped into a single level with an energy equal to the average energy of the states of that configuration. This is justified since both the atom and the electron densities of interest here are sufficiently high to ensure a strong collisional mixing between the populations in the levels of each configuration. The energy level diagrams of Ar and Ar_2^* have been taken from [26,30].

It is beyond the scope of this paper to present this collisional-radiative model in full detail since this would be too lengthy. Details can be found elsewhere [31]. Here, we will present only a brief summary of this model to illustrate, for the sake of consistency, how the data to be inserted in Eqs. (1) and (5) can be obtained.

The list of processes considered in the rate balance equations for the above species is given in Table I in a condensed manner. These include: ionization, excitation, reexcitation and deexcitation processes by electron impact, all the allowed radiative transitions, chemi-ionization, three-body and dissociative recombination, conversion of atomic ions into molecular ions, diffusion of metastables and charged species, and other processes. The total rate of ionization (2) is the

TABLE I. List of elementary processes taken into account in the collisional-radiative model and the electron Boltzmann equation.

Elastic scattering	$M+e \Rightarrow M+e$	$M=\mathrm{Ar},\mathrm{Ar}^+,\mathrm{Ar}_2^+,\mathrm{Ar}_3^+$
Excitation/deexcitation	$\mathrm{Ar}(k)+e \Leftrightarrow \mathrm{Ar}(m)+e$	$k,m=0,4s,4p,3d,5s,5p,4d,6s$
Ionization	$\mathrm{Ar}(k)+e \Rightarrow \mathrm{Ar}^+ + 2e$	$k=0,4s,4p,3d,5s,5p,4d,6s$
Three-body recombination	$\mathrm{Ar}_k^+ + e + \begin{Bmatrix} e \\ \mathrm{Ar} \end{Bmatrix} \Rightarrow \mathrm{Ar}(4p) + \begin{Bmatrix} e \\ \mathrm{Ar} \end{Bmatrix}$	$k=1,2,3$
Dissociative recombination	$\mathrm{Ar}_2^+ + e \Rightarrow \mathrm{Ar}(4p) + \mathrm{Ar}$ $\mathrm{Ar}_3^+ + e \Rightarrow \mathrm{Ar}(4p) + \mathrm{Ar}_2^*$	
Diffusion	$M \Rightarrow \mathrm{wall}$	$M=\mathrm{Ar}(4s),e,\mathrm{Ar}^+,\mathrm{Ar}_2^+,\mathrm{Ar}_3^+$
Spontaneous emission	$\mathrm{Ar}(k) \Rightarrow \mathrm{Ar}(m)+h\omega$ $\mathrm{Ar}_2^* \Rightarrow 2\mathrm{Ar}+h\omega$	all allowed transitions
Chemi-ionization	$\mathrm{Ar}(k)+\mathrm{Ar}(m) \Rightarrow \begin{cases} \mathrm{Ar}^+ + \mathrm{Ar} + e \\ \mathrm{Ar}_2^+ + e \end{cases}$	$\begin{cases} k,m=4s,4p \\ k=m=4s \end{cases}$
Molecular ion conversion	$\mathrm{Ar}^+ + 2\mathrm{Ar} \Rightarrow \mathrm{Ar}_2^+ + \mathrm{Ar}$ $\mathrm{Ar}_2^+ + 2\mathrm{Ar} \Rightarrow \mathrm{Ar}_3^+ + \mathrm{Ar}$ $\mathrm{Ar}_3^+ + \mathrm{Ar} \Rightarrow \mathrm{Ar}_2^+ + 2\mathrm{Ar}$	
Heavy-particle collisions	$\mathrm{Ar}(4s)+2\mathrm{Ar} \Rightarrow \mathrm{Ar}_2^* + \mathrm{Ar}$ $\mathrm{Ar}(4p)+2\mathrm{Ar} \Rightarrow \mathrm{Ar}(4s)+2\mathrm{Ar}$ $\mathrm{Ar}(4p)+\mathrm{Ar} \Rightarrow \mathrm{Ar}(4s)+\mathrm{Ar}$	

sum of the contributions of ionization from the atom ground and excited states and the dimer Ar_2^* [21], by electron impact, and from the various chemi-ionization processes. Ionization from the dimer is important under the present conditions since its population can be rather high. It is primarily formed by three-body collisions of $\mathrm{Ar}(4s)$ with two Ar atoms. The loss of electrons occurs through volume recombination with the atomic and the molecular ions, via three-body and dissociative recombination processes, respectively [total rate of recombination (3)], and ambipolar diffusion to the wall. Quasineutrality is assumed, that is, $n_e = [\mathrm{Ar}^+]+[\mathrm{Ar}_2^+]+[\mathrm{Ar}_3^+]$.

The electron Boltzmann equation has been solved using the two-term expansion in Legendre polynomials, taking into account all the electron elastic and inelastic processes listed in Table I as well as electron-electron collisions. For inert gases, the two-term expansion is accurate enough to determine the discharge properties under the present conditions. The solutions have been found in the local approach, that is, assuming that the electron energy distribution function (EEDF) is determined at each point by the local plasma parameters. Such an assumption is justified for the values of the gas density–tube radius product considered in this work (corresponding to pR values above 100 Torr cm), since the electron energy and momentum relaxation lengths are much smaller than the plasma radius in this case. In this case, the radial dependence of the EEDF is only due to the radial variations of the electron and the gas densities.

In the present treatment of the Boltzmann equation, we have assumed that the primary and the secondary electrons equally share the available energy after an electron impact ionization process. In the case of chemi-ionization processes, it was assumed that the energy of the outcoming electron is equal to the total energy available after the reaction. Finally, in what concerns recombination, effective electron energy-dependent recombination cross sections have been used that yield, upon integration over a Maxwellian distribution, values of recombination coefficients in agreement, both in magnitude and electron temperature dependence, with available data for argon.

In order to account approximately for the effects of diffusion losses on the EEDF, a diffusion term of the form $v_{\mathrm{diff}} f^0 u^{1/2}$ has been included in the Boltzmann equation, where

$$\nu_{\mathrm{diff}} n_e = \Gamma_{\mathrm{ion}} - \Gamma_{\mathrm{rec}} \tag{8}$$

is an effective diffusion frequency, assumed to be velocity independent, and the EEDF is normalized such that $\int_0^\infty u^{1/2} f^0(u,r)du = n_e(r)$, with u denoting the electron energy. The inclusion of such a term is necessary in order that the creation of secondary electrons exactly compensates for the electron losses, at each radial position, in the Boltzmann equation itself, consistently with the continuity equation (1) (recall that the latter is just a moment of the Boltzmann equation).

In most of the steady-state, homogeneous Boltzmann codes accounting for diffusion losses, the effective diffusion frequency is considered fixed and the strength of the applied field is varied until the creation-loss balance is fulfilled. In our case this method does not apply since we are dealing with a strongly inhomogeneous problem in which the effective diffusion frequency varies radially consistently with Eq. (8). This equation must be verified at every radial position. Further, the discharge maintenance field is to be determined here as an eigenvalue solution of the continuity equation (1) with the boundary conditions (4), not from the Boltzmann equation itself. For this reason, we used the following procedure (see Sec. IV for further details about the full numerical procedure): for any values of the external field strength used at intermediate calculation steps (as the iterations proceed towards convergence), the effective diffusion frequency at each radial position was varied until Eq. (8) was locally satisfied. In this way, when full convergence is achieved and the actual value of the maintenance field is found as the eigenvalue solution of Eq. (1), one can be sure that the so-

TABLE II. List of elementary processes taken into account for the calculation of the gas heating term Q [see Eq. (5) in the main text].

Elastic scattering	$Ar+e \Rightarrow Ar+e$
Elastic scattering	$Ar^{+}+e \Rightarrow Ar^{+}+e$
Elastic scattering	$Ar_2^{+}+e \Rightarrow Ar_2^{+}+e$
Elastic scattering	$Ar_3^{+}+e \Rightarrow Ar_3^{+}+e$
Molecular ion conversion	$Ar^{+}+2Ar \Rightarrow Ar_2^{+}+Ar$
Molecular ion conversion	$Ar_2^{+}+2Ar \Rightarrow Ar_3^{+}+Ar$

lutions of the Boltzmann equation across the tube and of the continuity equation are fully consistent with each other. Note, however, that at the pressures considered here the solutions of the Boltzmann equation are mostly determined by collisional processes, and are quite insensitive to the assumed form of the diffusion frequency.

The calculation of the gas heating source [term Q in Eq. (5)] takes into account all collisional processes that convert some energy into the gas translational mode. At the high pressures of interest here the mean free path of ion–neutral-species collisions (elastic and charge exchange collisions) is very small, therefore it was assumed that the gas and the ion temperatures are the same. Consistently with this assumption, the power transferred to the ions through elastic electron-ion collisions is to be considered as a direct source of gas heating. According to the model calculations, the major gas heating sources in our case are the elastic collisions of electrons with atoms and ions and the conversion processes of atomic into molecular ions listed in Table II.

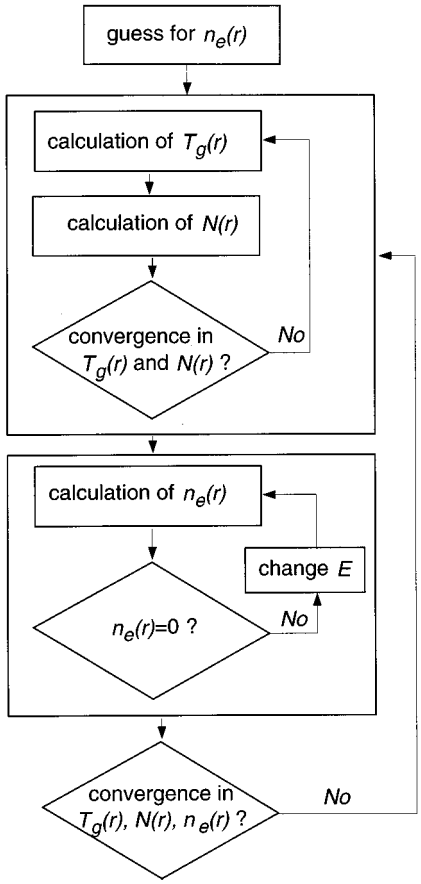

FIG. 1. Flowchart of the numerical solution.

IV. NUMERICAL APPROACH

A brief description of the numerical approach used to solve the system of equations is presented below. The electron continuity equation (1) has been discretized on a grid of appropriately chosen radial positions r_k, where k is an integer running from zero to a final value M. The number of grid points was typically between 20 and 40, depending on the particular situation. An equidistant grid $r_k=k\Delta r$, where $\Delta r=R/M$ is the step size, is appropriate for diffuse discharges and when the contraction is small. For moderately or highly contracted discharges, we used a nonequidistant grid, the grid points of which are concentrated in the center of the discharge. After discretization Eq. (1) takes the form

$$a_{k-1}y_{k-1}+a_k y_k+a_{k+1}y_{k+1}=b_k, \quad k=0,1,\ldots,M-1, \tag{9}$$

where $y_k=n_e(r_k)/n_e(0)$. Due to the symmetry $a_{-1}=a_1$ and $y_{-1}=y_1$. The boundary condition (4) reads $y_M=0$. The electron density at the axis is assumed as an input parameter. The electron density profile can be found from the relation

$$y_{k+1}=\begin{cases} \dfrac{b_k-a_k y_k}{2a_{k+1}}, & k=0, \\ \dfrac{b_k-a_{k-1}y_{k-1}-a_k y_k}{a_{k+1}}, & k=1,2,\ldots M-1 \end{cases} \tag{10}$$

with initial condition $y_0=1$. For any k, starting from the center, the right-hand side of Eq. (1), and hence of Eq. (9), can be calculated from the electron Boltzmann equation. For arbitrary choices of the electric field E the solution of Eq. (1) may diverge or swing to unphysical negative values of the electron density. This is because not all values E lead to physically acceptable solutions. In particular, the boundary condition at $r=R$ can be satisfied only for one particular value of E. Indeed, as is well known Eq. (1) with the conditions (4) constitutes an eigenvalue problem the solution of which involves the determination of one eigenvalue. This eigenvalue is the steady-state maintaining field E in the present case. This situation holds of course for both diffuse and contracted discharges.

The approach used to solve Eq. (5) with the boundary conditions (6) consists of discretizing both Eqs. (5) and (6). With this approach, a tridiagonal matrix is obtained, which can easily be solved using standard numerical techniques to obtain the radial distribution of the gas temperature. The radial distribution of the atom density is then directly obtained from Eq. (7). However, since the right-hand side of Eq. (5) depends on the atom density, which in turn depends on the gas temperature through Eq. (7), a few iterations are necessary to get convergence.

The numerical approach used to solve our system of equations is schematically represented by the flowchart in Fig. 1. The calculations start with a guess for the electron density profile. For a fixed electron density profile, Eqs. (5) and (7),

with the boundary conditions (6), are iteratively solved until both $T_g(r)$ and $N(r)$ converge. After this, Eq. (1) is solved as an eigenvalue problem in the way explained above. Starting with a guess for the electric field, this equation is iteratively integrated from the center to the wall for successive values of the electric field until the electron density at the wall matches the boundary condition. This numerical procedure cannot ensure an exact mathematical fulfillment of the condition $n_e(R)=0$ unless the iterations proceed over a prohibitive period of time. For this reason, in practice it is sufficient to require the electron density at the wall to be about two orders of magnitude smaller than that at the axis. This suffices to determine the eigenvalue to within a high accuracy (see further below). While solving Eq. (1), the radial distribution of both the gas temperature and atom density remains unchanged. Having found the radial distribution of the electron density, Eqs. (5) and (7) are solved again for this distribution to determine corrected radial distributions of the gas temperature and density. Then, Eq. (1) must be solved again. Usually, three or four iterations suffice to converge all the distributions.

The above solution procedure requires the following input parameters: the tube radius, the gas pressure at the room temperature (300 K), and the electron density at the axis. Since the discharge current and the electron density at the axis are uniquely related, it is better to take the latter density as an input parameter. The current can be determined afterwards from the calculated radial distributions of the electron density and drift velocity.

The procedure described above is a double loop. In each external loop the eigenvalue problem must be solved. The eigenvalue determination is a loop too, in which Eq. (1) must be solved several times until the boundary condition is fulfilled. But, to find a solution to Eq. (1) requires solving the kinetic model equations and the Boltzmann equation several times in order to obtain the right-hand-side term b_k and the coefficients a_k of Eq. (9). This poses severe difficulties concerning the computation time, which can be, however, somewhat overcome by choosing a nonequidistant grid.

The main difficulty of the whole numerical algorithm is the sensitivity of the eigenvalue determination. For low electron densities at the axis, only a couple of iterations suffice to obtain the value of the electric field. For elevated, on-axis electron densities, determination of the electric field is more sensitive and requires a higher precision. Usually, a precision of about $10^{-3}-10^{-4}$ was enough, but sometimes a precision of 10^{-6} turned out to be necessary. For high axial electron densities, even very small changes in the electric-field strength may cause dramatic changes in the solution and lead to unphysical solutions (for example, with negative values of the electron density in some regions across the tube), so that many iterations are then necessary to determine this eigenvalue. Moreover, in this case the electron Boltzmann equation must be solved with much higher precision also, which becomes more and more difficult with increasing electron densities. Nevertheless, the system was found to be physically stable and, as expected, a unique physical solution could been determined in all cases investigated.

We found that numerical difficulties may also arise even for moderate axial electron densities, because the right-hand side of Eq. (1) changes its sign at some intermediate radial position. Near the discharge axis this term is always positive, while near the wall it becomes negative when constriction occurs (see Fig. 5). Such a change of sign has been mentioned by several authors and can easily be explained. It is due to the strong nonlinear dependence of the ionization rate on the electron density, which makes this rate decrease much faster and become smaller than the recombination rate in the outer plasma regions of the constricted column. Another source of numerical difficulties is that the right-hand side of Eq. (1) is the difference of two terms (the ionization and the recombination rates) which can both be very large near the axis, but nearly compensate each other, as the electron density increases. Their difference is a much smaller term the determination of which can cause numerical instabilities when solving Eq. (1).

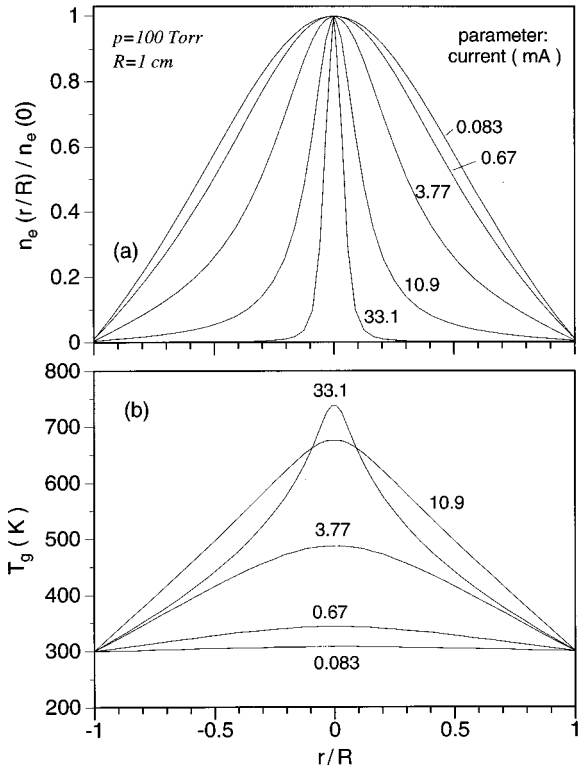

FIG. 2. Radial distribution of the normalized electron density (a) and of the gas temperature (b) for a pressure of 100 Torr, a tube radius of 1 cm, and different discharge currents.

V. RESULTS AND DISCUSSION

Let us first present typical results concerning the transition from the diffuse to the contracted mode and the main plasma parameters in both regimes. Comparisons are made with experimental data when available.

Figure 2(a) shows the transition from the diffuse to the constricted discharge as the current increases, for $p=100\,\mathrm{Torr}$ and $R=1\,\mathrm{cm}$. For the currents considered, the electron density at the axis varies from 10^9 to $10^{13}\,\mathrm{cm}^{-3}$ [Fig. 7(a) shows a plot of the on-axis electron density *versus* current under the present conditions]. When increasing the discharge current up to about 1 mA the radial distribution of the electron density is little changed and remains close to the

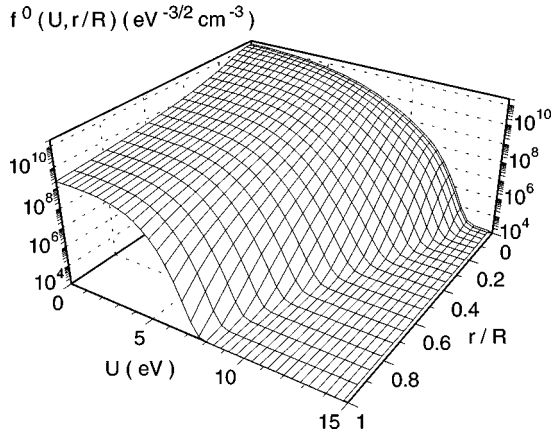

FIG. 3. Electron energy distribution function at various normalized radial positions r/R, for a pressure of 100 Torr, a tube radius of 1 cm and a discharge current of 10.9 mA.

typical profile of the fundamental diffusion mode in cylindrical geometry. The actual distributions are just a little narrower than the classical Bessel profile, as one can assess by using the parameter $\xi=\bar{n}_e/n_e(0)$, where $\bar{n}_e=\int_0^R 2\pi r n_e(r)dr/(\pi R^2)$ is the mean electron density across the radius, as a measure of the constriction. In fact, we have $\xi=0.38$ and $\xi=0.34$ for $I=83\,\mu$A and $I=0.67$ mA, respectively ($\xi=0.43$ for the Bessel profile). The constriction onsets near 4 mA, with a pronounced contraction of the radial profile occurring over the limited current range of 4–10 mA. For $I>10$ mA, the constriction still continues, but at a slower rate. The critical current value for the transition is, therefore, about 4 mA in the present case.

Figure 2(b) shows the radial distribution of the gas temperature for the same discharge parameters as Fig. 2(a). As expected, the gas temperature at the axis and over the whole cross section increases with the discharge current, and gas heating can become quite considerable. Significant deviations from the room temperature start to appear for currents a little lower than 1 mA, before the constriction begins. This seems to indicate that gas heating plays some role in the constriction process, but the actual importance of this effect will have to be further investigated below.

Figures 3–6 show the radial distributions of several plasma parameters of interest in a constricted discharge, for $p=100$ Torr, $R=1$ cm, and $I=10.9$ mA. The calculated discharge maintenance field under such conditions is 42.2 V/cm and the input power per unit length is 0.460 W/cm. The EEDF at several radial positions is presented in Fig. 3 to illustrate the spatial behavior of this distribution. For simplicity, this figure shows values of the EEDF greater than $10^3\,\mathrm{eV}^{-3/2}\,\mathrm{cm}^{-3}$ only. With this representation, the figure shows about seven decades of variation of the EEDF at the axis, and approximately five decades near the wall. The degree of ionization varies from approximately 10^{-6}, at the discharge axis, to approximately 10^{-8}, near the wall. We note that the EEDF's near the wall and at the axis differ significantly in shape. This is due to the different gas and electron densities at both locations. Due to the small degrees of ionization, electron-electron collisions have some effect on the EEDF shape only in the central region and the distribution is far from a Maxwellian everywhere. The radial

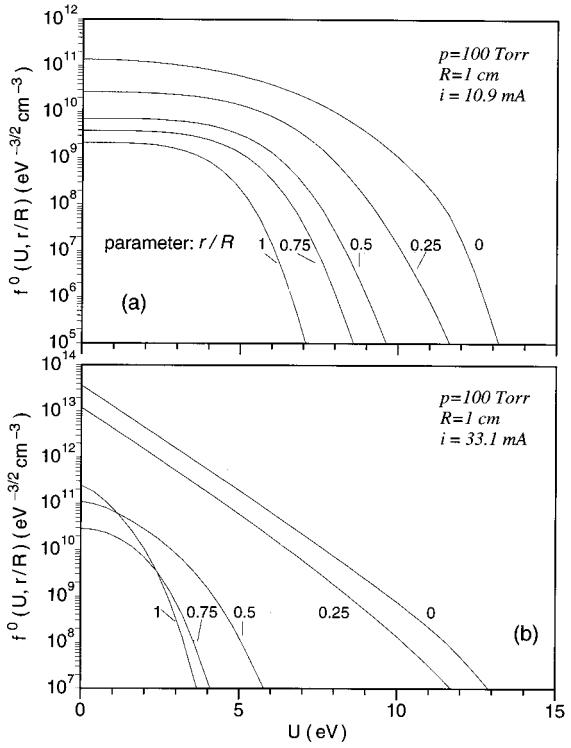

FIG. 4. Electron energy distribution function at several normalized radial positions r/R, for a pressure of 100 Torr, a tube radius of 1 cm, and discharge currents of 10.9 mA (a) and 33.1 mA (b).

change in the EEDF shape mostly reflects the E/N scaling of the distribution in this case.

Maxwellization effects due to electron-electron collisions are illustrated in Fig. 4 showing the EEDF at different radial positions, for $I=10.9$ and 33.1 mA. The EEDF becomes closer to a Maxwellian with increasing discharge current, but the extension of this effect depends on the radial position since the degree of ionization decreases toward the wall. For $I=33.1$ mA, the body of the EEDF is nearly Maxwellian in the center, while it is more Druyvesteyn-like shaped in the outer regions.

Figure 5 shows the radial distributions of the electron, the ion, and the excited-state concentrations. From the axis outwards, the electron density falls by a factor of approximately 10 over a distance $r/R\approx0.3$, which indicates considerable constriction. While for the usual Bessel density profile $\xi\approx0.43$, in the present situation $\xi=0.0415$. The density of Ar^+ ions also changes drastically across the radius. This density peaks at the axis with a value of approximately one eighth of the electron density, but decreases much faster than the electron density with increasing radius. Everywhere across the tube, Ar_2^+ is the dominant ion, its density representing approximately 98% of the total density of all the ion species, except in a very narrow central channel. The density of Ar_2^+ is approximately two orders of magnitude smaller then that of Ar_2^+, so this ion has no influence on the discharge kinetics. On the basis of the above results, a simplified set of ion kinetics can be suggested. To a first approximation, it would be sufficient to consider only Ar_2^+ ions and assume that all atomic ions formed by electron collisions and chemi-ionization reactions are immediately converted into

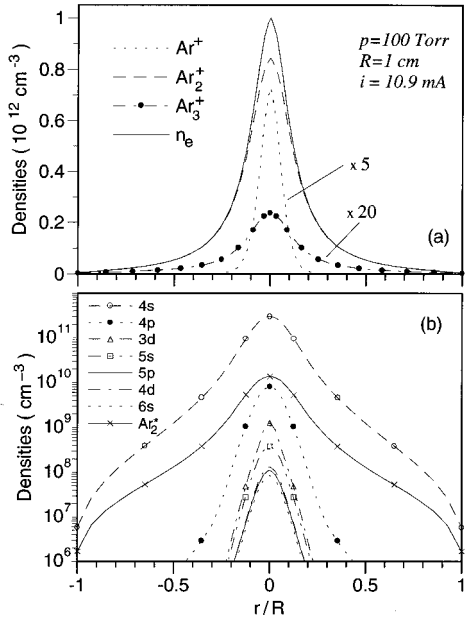

FIG. 5. Radial distribution of the electron and ion densities (a) and of the populations of the excited states (b) for the discharge conditions of Fig. 3. The density of Ar^+ is multiplied by factor of 5 and that of Ar_3^+ by factor of 20.

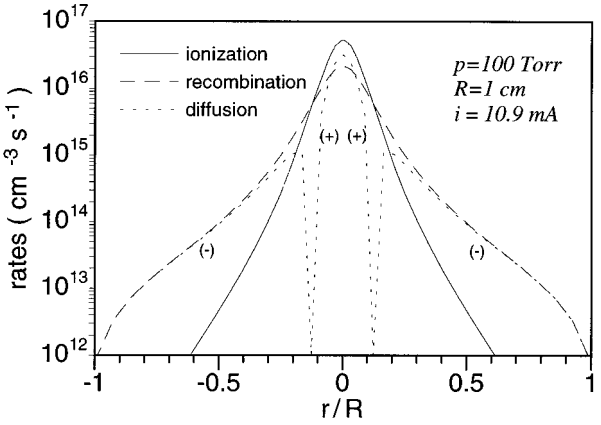

FIG. 6. Radial distributions of the ionization, recombination and diffusion rates. The symbols (+) and (−) denote the positive and the negative branches of the diffusion rate, respectively. The discharge conditions are the same as in Fig. 5.

Ar_2^+ through three-body reactions (see Table I). Such an approximation would not much affect the recombination kinetics since dissociative recombination of electrons with Ar_2^+ ions overwhelms the other recombination processes under the present conditions.

As seen from Fig. 5(b), the population of the Ar($4s$) configuration largely exceeds that of any other configuration. This is principally due to the quasimetastable nature of this configuration (remind that two levels of this configuration are true metastables, while the other two are radiative states that behave like pseudometastables at these high pressures due to imprisonment of the resonance radiation). The mean populations of all higher configurations follow a pseudoequilibrium law with an excitation temperature considerably lower than that of the electrons. This is indicative of important radiative losses. The large difference between the populations of the first and the higher configurations occurs only for the moderate electron densities of this example (10^{10}–$10^{12}\,cm^{-3}$). In fact, for electron densities of about $10^{14}\,cm^{-3}$, the populations of the Ar($4p$) and the higher configurations become closer to that of Ar($4s$), and the excitation temperature closer to the electron temperature. Note also that the population of the molecular dimer Ar_2^* is very high so that, according to our results, this dimer cannot be disregarded in the model.

Figure 6 shows the radial distributions of the ionization and the recombination rates, and of their difference, that is, the net diffusion rate. To understand the behavior of these distributions, recall that the radial distribution of the atom density is nonuniform, due to gas heating. In the present case, the calculated gas temperature at the axis is 676 K (see Fig. 2), hence the gas density is about two times lower, and the reduced field E/N about two times higher, at the axis than at the wall. The electron density is also much higher at the axis than at the wall. Due to both of these reasons, the ionization rate, which is a strongly nonlinear function of the electron density and E/N, sharply peaks at the axis. On going from the axis to the wall, the decrease in electron density is about two orders of magnitude, while the ionization rate falls off by more than four orders of magnitude. On the other hand, the outward decrease in the recombination rate is much slower. In the center of the discharge the ionization rate is somewhat higher than the recombination rate, so that the difference between these two rates is balanced by a positive diffusion rate (corresponding to a net loss of electrons by diffusion, per unit volume). However, the ionization and the recombination rates exactly balance each other at a point not far from the axis due to the much sharper outward decrease of the former rate. Beyond this point, recombination overcomes the creation of new electrons, and a negative diffusion rate has to compensate for the difference (a negative diffusion rate means that the number of electrons diffusing into a given volume element is larger than that of those diffusing out of this element, per unit time; in this case, diffusion leads to a net gain of electrons, contrary to the usual situation where it leads to a net loss). As seen from Fig. 6, for $r/R > 0.3$ the recombination is balanced mainly by diffusion. The fact that recombination must be balanced by diffusion outside the constricted channel has been pointed out by several authors [4,6,7,10].

Detailed calculations similar to those presented above for 100 Torr argon pressure and $R=1$ cm have also been carried out for 200 and 500 Torr, and the same tube radius. Qualitatively, the basic trends of the calculated data are similar at all these pressures, but the values of the plasma parameters as a function of the current change of course with pressure. To illustrate this, Figs. 7 and 8 show calculated values of the electron density, electron temperature, and gas temperature at the tube axis, and of the maintenance electric field *versus* the discharge current, for 100 and 200 Torr argon pressure, respectively. Also shown in these figures for comparison are data inferred from experiments [14] for the same pressures, tube radius, and wall temperature (300 K) as the calculations. The diagnostics used in these experiments consisted of mea-

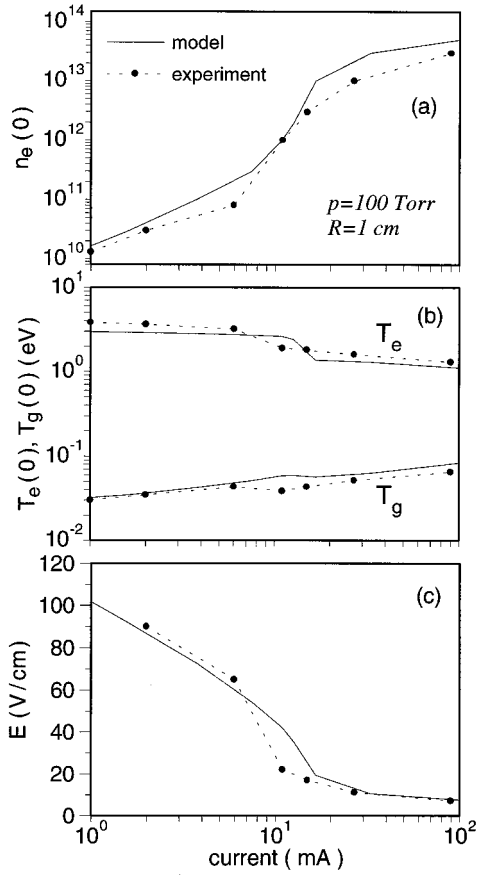

FIG. 7. Variation of the electron density (a) and the electron and the gas temperatures (b) at the discharge axis, and of the maintaining electric field (c) with the discharge current. The gas pressure is 100 Torr and the tube radius is 1 cm. Data points are from experiments in Ref. [14].

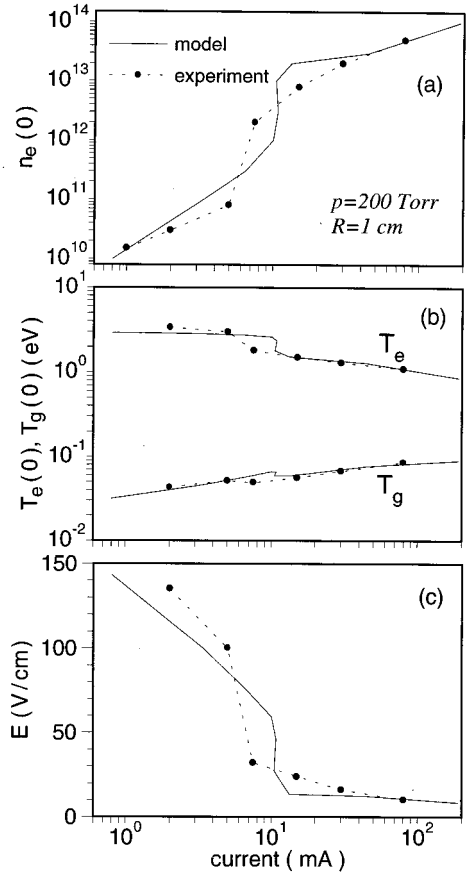

FIG. 8. As in caption to Fig. 7, but for a gas pressure of 200 Torr.

surements of the electric field and of the radial profile of the brightness of the bremsstrahlung continuum. From these measurements, the absolute values and radial profiles of the electron density and the atomic temperature have been determined in [14] using the current balance and the heat balance equations (assuming in the latter equation that all the discharge electrical power is transferred into gas heating), while the electron temperature was calculated from the measured electric field and the electron energy balance. Unfortunately, the errors associated with such determinations have not been estimated in [14].

Taking into account the various sources of error in the calculations (especially, the lack of accurate data for a number of kinetic processes) and in the data from experiments (indirect determinations based on model assumptions), one can conclude that the predictions of our model agree very satisfactorily, both in magnitude and in the basic trends of the various quantities, with the data given in [14]. There seems to exist, however, some discrepancy between theory and experiment as to the nature of the transition from the diffuse to the constricted mode (smooth or abrupt) and the corresponding critical current. This point deserves therefore further investigation.

The calculations shown in Figs. 7 and 8 reveal that the axial values of the electron density, electron temperature, and gas temperature, and the value of the electric field exhibit a jump for some critical value of the discharge current. In particular, the central value of the electron density suddenly increases, while the electron temperature and the maintenance field suddenly drop at some critical current value. Such jumps are also experimentally observed, even though the theoretical and experimental critical currents differ a little as it can be seen from these figures.

Although the existence of a critical current is well reproduced by the theory, the calculated plasma parameters for 100 Torr shown in Fig. 7, are single-valued functions of the current (in contrast with the results of the analytical model of Ref. [10]), thus the experimentally observed hysteresis effects [14] associated with constriction cannot be fully understood in terms of such plots. This is because the discharge current is not a proper physical parameter determining the plasma properties. The proper parameter is the power deposited in the plasma or, in the case of an axially uniform plasma column, the power deposited per unit column length (the specific power). Figure 9 shows that both the calculated and the experimental central electron density and temperature, and discharge maintenance field at 100 Torr argon pressure (same experimental data as in Fig. 7, but plotted now *versus* the specific power *EI*) are multivalued functions of the discharge specific power within some range of values of the latter. The calculated and the experimental data have the same qualitative trends: the density is an S-shaped function of the specific power, while the temperature and the electric

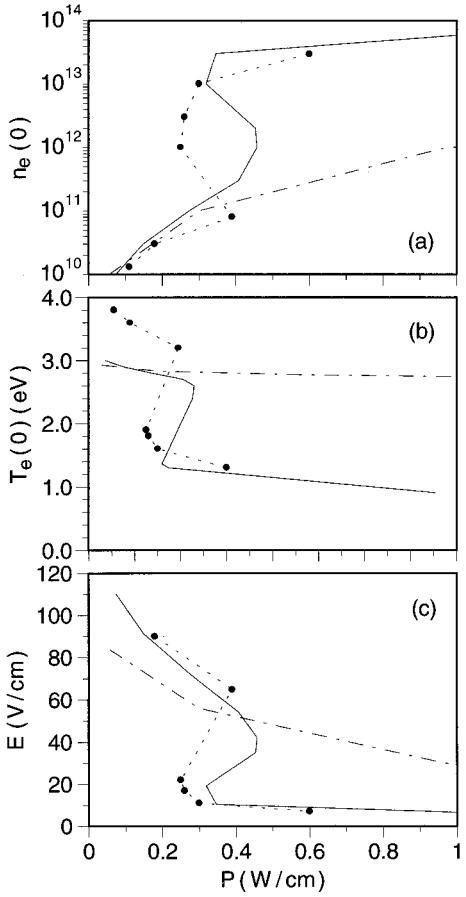

FIG. 9. Electron density and temperature at the discharge axis, and discharge maintenance field as a function of the electric power deposited per unit column length, for 100 Torr argon pressure and a tube radius of 1 cm. Solid curve, calculations using the complete model; data points, experiment; chain curve, calculations neglecting electron-electron collisions.

field are Z-shaped functions of the same parameter. Note that the discrepancies between theory and experiment in Fig. 9 just mirror in this plot those existing in Fig. 7. Similar S and Z shapes have also been found for the other pressures investigated, namely, 200 and 500 Torr. Such multivalued solutions explain the observed abrupt changes in the plasma parameters and the hysteresis as previously discussed by Golubovskii and co-workers [10–12].

The model investigated in this paper accounts for all processes that have been referred to in the literature as possible causes of constriction, namely, nonuniform gas heating, diffusion-recombination balance in the outer plasma column regions, and the strong radial decay of the ionization rate, which is connected with the importance of stepwise ionization processes and electron-electron collisions. It is, therefore, necessary to investigate further the importance of such processes by detailed simulations in order to get kinetic insight into the relevant processes.

Figure 10 compares the electron density profile obtained from the complete model with that obtained ignoring gas heating, that is, assuming a constant temperature of 300 K across the tube, for $p=100\,\mathrm{Torr}$, $R=1\,\mathrm{cm}$, and $I=14.7\,\mathrm{mA}$. It is seen that the discharge contracts even for a

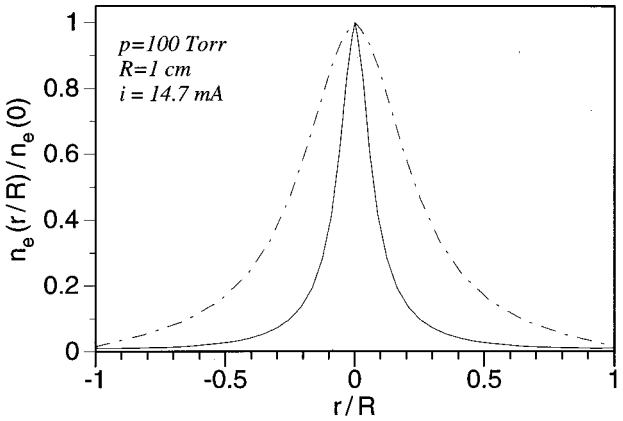

FIG. 10. Radial profile of the electron density in argon taking into account (solid curve) and neglecting (chain curve) gas heating, for 100 Torr pressure, a tube radius of 1 cm, and a discharge current of 14.7 mA. The central electron density is $2\times10^{12}\,\mathrm{cm}^{-3}$ in the former case and $5.2\times10^{11}\,\mathrm{cm}^{-3}$ in the latter one.

constant gas temperature, but that nonuniform gas heating contributes to additional contraction for given operating conditions. The simulations further show that, for constant gas temperature, sudden jumps in the discharge parameters and hysteresis also occur, but at a considerably higher critical current. Therefore, nonuniform heating of the gas is not a determining factor for the constriction phenomenon. This conclusion invalidates all earlier explanations of constriction as a direct consequence of nonuniform gas heating [1–3,13] (see Sec. I).

To illustrate further the gas heating effects, and also the role of electron-ion dissociative recombination, Fig. 11 shows results of simulations assuming a recombination rate about two orders of magnitude smaller and a thermal conductivity much higher than the corresponding values for argon (in fact, the values adopted for both parameters correspond to those of helium). Also shown for comparison are results for the same low recombination rate and constant gas temperature. In this latter case, due to the assumed, small value of the recombination rate, the ionization rate exceeds the recombination rate across the entire column cross section and is balanced primarily by diffusion losses. Therefore, the discharge is diffuse and no contraction is observed. However, as can be seen from this figure considerable contraction arises by considering gas heating, even though the high thermal conductivity assumed prevents strong gas heating in this case. Although small, the radial decrease of the gas temperature (consequently, the radial increase of the gas density) suffices to cause a decrease of the ionization rate with radius that is fast enough for this rate to become smaller than the recombination rate in the outer plasma regions. This triggers sudden contraction of the discharge. Such a rapid variation is due to the complex nonlinear dependence of the ionization rate on the degree of ionization (through cumulative ionization processes and the influence of electron-electron collisions on the shape of the EEDF) and the reduced maintenance field E/N.

The results in Figs. 10 and 11 reveal that the occurrence of sudden contraction must be connected with the strongly

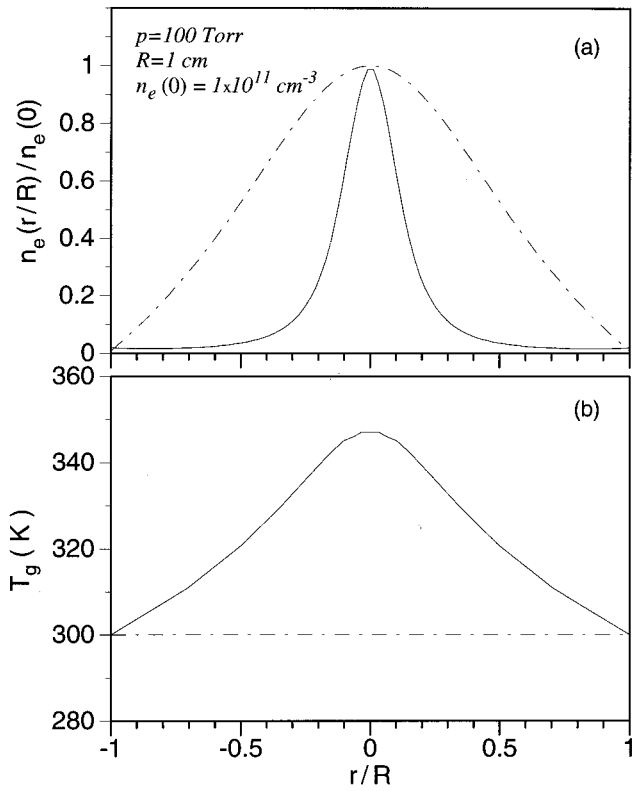

FIG. 11. Calculated radial distributions of the electron density (a) and the gas temperature (b) when the values of the dissociative recombination rate and the gas thermal conductivity of argon are replaced with those of helium, for a pressure of 100 Torr, a tube radius of 1 cm and a central electron density of $10^{11}\,\mathrm{cm}^{-3}$ (solid lines). Also shown for comparison are similar calculations, but assuming a constant gas temperature of 300 K across the tube (chain lines). The discharge current is 3.8 mA in the former case and 7.5 mA in the latter one.

nonlinear variations of the ionization rate referred to above. As a final step, we need to elucidate which nonlinear mechanisms play a key role. To this end, a simulation was performed using our full model for 100 Torr argon pressure but ignoring electron-electron collisions in the Boltzmann equation (thus, still taking into account gas heating and cumulative ionization processes). In this case, a continuous contraction of the density profile takes place with increasing current but no abrupt changes in the plasma parameters and hysteresis do occur as shown in Fig. 9. This confirms the conclusions drawn by Golubovskii and co-workers [10–12] from simplified analytical models about the key role played by electron-electron collisions in constriction phenomena in argon.

VI. CONCLUSIONS

A numerical model based on solutions of the electron continuity equation and the gas thermal balance equation, coupled to the electron Boltzmann equation and to a collisional-radiative model for the dominant neutral and ion species, has been developed to investigate the properties of dc discharges in argon at high pressures and the mechanisms of constriction. To our knowledge, this is the first time that the constriction phenomenon in argon is quantitatively analyzed on the basis of a complete, self-consistent discharge model. The model quantitatively reproduces the observed evolution of the discharge parameters as the current increases at fixed pressure, the occurrence of abrupt changes in the values of such parameters at some critical current, and hysteresis. These abrupt changes and the hysteresis, which are associated with constriction, have been shown to be due to the fact that the plasma parameters become multivalued functions of the specific electrical power deposited into the discharge within a limited range of values of the latter, above some critical value. The existence of multivalued solutions of the internal plasma parameters *versus* the power load (external parameter) indicates that the mechanisms of constriction in dc and microwave discharges can presumably be understood within the same theoretical framework.

Kinetic insights on the relevant processes of constriction are provided by the present model for argon, which are instrumental to understand also constriction phenomena in other situations. It was shown that gas heating, cumulative ionization, and the influence of electron-electron collisions in forming the distribution function contribute altogether to contraction and must be taken into account to explain quantitatively the observations. However, it was demonstrated that nonuniform gas heating and cumulative ionization cannot explain the occurrence of sudden contraction and hysteresis. Only the complex dependence of the ionization rate on the degree of ionization through the effects of electron-electron collisions on the electron energy distribution function can explain such phenomena. In fact, we have shown that in the absence of such collisions the discharge contracts as the power load increases, but no sudden changes in the discharge parameters or hysteresis occur. On the other hand, taking into account the effects of electron-electron collisions but assuming a constant gas temperature in the model, sudden contraction and hysteresis still occur but for critical currents far above the experimental values. Though as noted above inhomogeneous gas heating is not responsible for sudden contraction and hysteresis, the radial decay of the gas temperature enhances the contraction and contributes to decrease the critical current towards the observed values.

In conclusion, our model invalidates previous works in which constriction is attributed to nonuniform gas heating [1–3,13], but confirms on solid grounds the explanations proposed in Refs. [10–12] on the basis of simplified models. This model provides, therefore, clear-cut conclusions regarding existing controversies in the literature about the mechanisms of constriction.

Future work should lead to the development of appropriate collisional-radiative models for other gases and investigate constriction in other types of discharges, following the basic guidelines of this paper.

ACKNOWLEDGMENTS

One of us (G.P.) would like to thank NATO for financial support. This work was supported by the Portuguese Ministry of Science and Technology in the framework of the PRAXIS XXI Progamme, partially funded by the Programme FEDER of the European Union.

[1] C. Kenty, Phys. Rev. **126**, 1235 (1962).
[2] J. T. Massey and S. M. Cannon, J. Appl. Phys. **36**, 361 (1965).
[3] J. T. Massey, J. Appl. Phys. **36**, 373 (1965).
[4] A. V. Eletskii and B. M. Smirnov, Zh. Tekh. Fiz. **40**, 1682 (1970) [Sov. Phys. Tech. Phys. **15**, 1308 (1971)].
[5] K. N. Ul'yanov, Zh. Tekh. Fiz. **43**, 570 (1973) [Sov. Phys. Tech. Phys. **18** (3), 360 (1973)].
[6] Yu. B. Golubovskii, A. K. Zinchenko, and Yu. M. Kagan, Zh. Tekh. Fiz. **47**, 1478 (1977) [Sov. Phys. Tech. Phys. **22(7)**, 851 (1977)].
[7] Yu. B. Golubovskii and R. Lyagushchenko, Zh. Tekh. Fiz. **47**, 1852 (1977) [Sov. Phys. Tech. Phys. **22**(9), 1073 (1977)].
[8] Yu. B. Golubovskii and R. Sonneburg, Zh. Tekh. Fiz. **49**, 754 (1979) [Sov. Phys. Tech. Phys. **24** (4), 437 (1979)].
[9] Yu. B. Golubovskii and R. Sonneburg, J. Phys. Colloq. **40**, C7-155 (1979).
[10] Yu. B. Golubovskii and R. Sonneburg, Zh. Tekh. Fiz. **49**, 302 (1979) [Sov. Phys. Tech. Phys. **24** (2), 177 (1979)].
[11] Yu. B. Golubovskii, V. O. Nekuchaev, and E. B. Pelyukova, Zh. Tekh. Fiz. **66**, 43 (1996) [Tech. Phys. **41** (3), 254 (1996)].
[12] Yu. B. Golubovskii, V. O. Nekuchaev, and E. B. Pelyukova, Zh. Tekh. Fiz. **66**, 76 (1996) [Tech. Phys. **41** (10), 1011 (1996)].
[13] V. Yu. Baranov and K. N. Ul'yanov, Zh. Tekh. Fiz. **39**, 249 (1969) [Sov. Phys. Tech. Phys. **14** (2), 176 (1969)]; **39**, 259 (1969) [**14** (2), 183 (1969)].
[14] Yu. B. Golubovskii and R. Sonneburg, Zh. Tekh. Fiz. **49**, 295 (1979) [Sov. Phys. Tech. Phys. **24** (2), 173 (1979)].
[15] E. I. Toader, J. Phys. D **28**, 75 (1995).
[16] M. Moisan, R. Pantel, and J. Hubert, Contrib. Plasma Phys. **30**, 293 (1990).
[17] M. D. Calzada, M. Moisan, A. Gamero, and A. Sola, J. Appl. Phys. **80**, 46 (1996).
[18] G. L. Rogoff, Phys. Fluids **15**, 1931 (1972).
[19] P. G. Daniels, R. N. Franklin, and J. Snell, J. Phys. D **23**, 823 (1990).
[20] D. B. Ogle and G. A. Woolsey, J. Phys. D **20**, 453 (1987).
[21] P. K. Milson, J. Phys. D **29**, 403 (1996).
[22] C. G. Braun and J. A. Kunc, Phys. Fluids **30**, 499 (1987).
[23] J. Bretagne, J. Phys. D **14**, 1225 (1981).
[24] J. Bretagne, J. Godart, and V. Puech, J. Phys. D **15**, 2205 (1982).
[25] C. M. Ferreira, J. Loureiro, and A. Ricard, J. Appl. Phys. **57**, 82 (1985).
[26] S. Neeser, T. Kunz, and H. Langhoff, J. Phys. D **30**, 1489 (1997).
[27] E. Elson and M. Rokni, J. Phys. D **29**, 716 (1996).
[28] J. Vlcek, J. Phys. D **22**, 623 (1989).
[29] J. Vlcek and V. Pelikan, J. Phys. D **22**, 632 (1989).
[30] C. M. Ferreira and J. L. Delcroix, J. Appl. Phys. **49**, 2380 (1978).
[31] G. Petrov and C. M. Ferreira (unpublished).